

# Thanks for Nothing: Predicting Zero-Valued Activations with Lightweight Convolutional Neural Networks

Gil Shomron<sup>1</sup> Ron Banner<sup>2</sup> Moran Shkolnik<sup>1,2</sup> Uri Weiser<sup>1</sup>

Technion — Israel Institute of Technology<sup>1</sup>

Intel — Artificial Intelligence Products Group (AIPG)<sup>2</sup>

{gilsho@tx, uri.weiser@ee}.technion.ac.il {ron.banner, moran.shkolnik}@intel.com

## Abstract

Convolutional neural networks (CNNs) introduce state-of-the-art results for various tasks with the price of high computational demands. Inspired by the observation that spatial correlation exists in CNN output feature maps (ofms), we propose a method to dynamically predict whether ofm activations are zero-valued or not according to their neighboring activation values, thereby avoiding zero-valued activations and reducing the number of convolution operations. We implement the zero activation predictor (ZAP) with a lightweight CNN, which imposes negligible overheads and is easy to deploy and train. Furthermore, the same ZAP can be tuned to many different operating points along the accuracy-savings trade-off curve. For example, using VGG-16 and the ILSVRC-2012 dataset, different operating points achieve a reduction of 23.5% and 32.3% multiply-accumulate (MAC) operations with top-1/top-5 accuracy degradation of 0.3%/0.1% and 1%/0.5% without fine-tuning, respectively. Considering one-epoch fine-tuning, 41.7% MAC operations may be reduced with 1.1%/0.52% accuracy degradation.

## 1. Introduction

In the past decade, convolutional neural networks (CNNs) have been adopted for numerous applications [40, 37, 25], introducing state-of-the-art results. Despite being widely used, CNNs involve a considerable amount of computations. For example, classification of a 224x224 colored image requires billions of multiply-accumulate (MAC) operations [3, 43]. Such computational loads have many implications, from execution time to power and energy consumption of the underlying hardware.

CNN output feature maps (ofms) have been observed to exhibit spatial correlation, *i.e.*, adjacent ofm activations share close values [31, 39]. This observation is particularly true for zero-valued activations, as it is common practice to

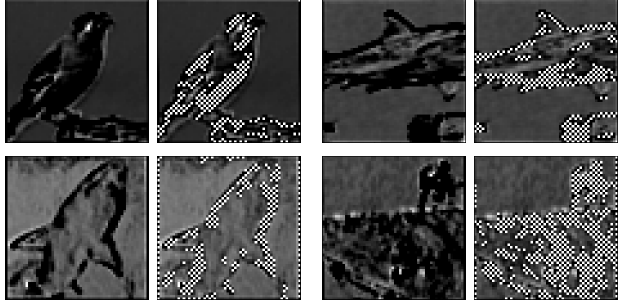


Figure 1: Exploiting spatial correlation for zero-value prediction of ofm activations with CNN-based predictor. Bright white pixels represent a predicted zero-valued ofm activation.

use the ReLU activation function [32], which squeezes all negative values to zero. If it were possible to predict which of the convolution operations will result in a negative value, they could be skipped, their corresponding ofm activations could be set to zero, and many multiply-accumulate (MAC) operations could be saved, which in turn may also save energy.

Prediction mechanisms are at the heart of many general-purpose processors (GPPs), leveraging unique application characteristics, such as code semantics and temporal locality, to predict branch prediction outcomes and future memory accesses, for example. Prediction mechanisms may similarly be employed for CNNs. In this paper, we propose a prediction method for CNNs that dynamically classifies ofm activations as zero-valued or non-zero-valued by leveraging the spatial correlation of ofms. The zero activation predictor (ZAP) works in three-steps: first, only a portion of the ofm is fully computed; then, the remaining activations are classified as zero-valued or non-zero-valued using a lightweight convolutional neural network; and finally, the predicted non-zero-valued activations are computed while the zero-valued activations are skipped, thereby saving entire convolution operations (Figure 1). ZAP imposes neg-

ligible overheads in terms of computations and memory footprint, it may be plugged into pretrained models, and is trained quickly and in parallel. In addition, ZAP’s speculation level is tunable, enabling different operating options according to existing constraints.

Model pruning is a related concept. With pruning, parameters [12, 27] and activations [28, 14] are classified as insignificant with the goal of discarding them. Pruning strategies commonly include retraining phases, since accuracy decreases after the model is trimmed. Increased model sparsity, when accompanied with the appropriate hardware [2, 11, 33, 38], leads to a decrease in MAC operations. As opposed to pruning, our method focuses strictly on the zero-valued ofm activations; therefore, ZAP can capture a range of operating points that does not require retraining. That said, pruning may be a byproduct of ZAP when set to high speculation levels, as misprediction of non-zero-valued activations as zero-valued is practically pruning. Interestingly, we observe that these mispredictions usually occur with small activation values; therefore, ZAP may also act as a pruning strategy, in which case we also introduce minor fine-tunings.

This paper makes the following contributions:

- **Zero activation predictor (ZAP).** We introduce a dynamic, easy to deploy, CNN-based zero-value prediction method that exploits the spatial correlation of output feature map activations. Compared with conventional convolution layers, our method imposes negligible overheads in terms of both computations and parameters.
- **Trade-off control.** We estimate the model’s entire accuracy-to-savings trade-off curve with mostly local statistics gathered by each predictor. This provides a projection of the model and the predictor performance for any operating point.
- **Accuracy to error linearity.** We show, both analytically and empirically, that the entire model accuracy is linear with the sum of local misprediction errors, assuming they are sufficiently small.

## 2. ZAP: Zero Activation Predictor

In this section, we describe our prediction method and its savings potential. We analyze its overheads in terms of computational cost and memory footprint and show that both are negligible compared with conventional convolution layers.

### 2.1. Preliminary

A convolution layer consists of a triplet  $\langle X_i, X_o, W \rangle$ , where  $X_i$  and  $X_o$  correspond to the input and output activation tensors, respectively, and  $W$  corresponds to the set

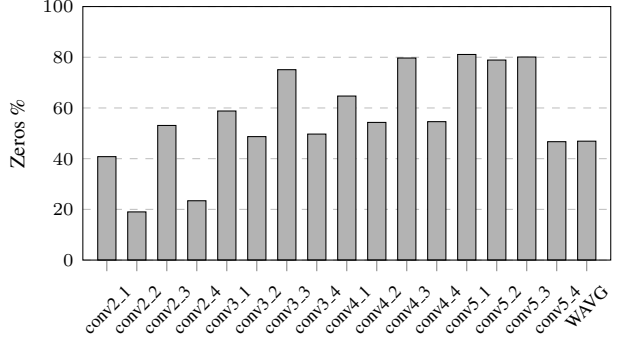


Figure 2: ResNet-18 ofm sparsity as measured across the entire ILSVRC-2012 validation set. Each bar represents the relative portion of zero-valued ofm activations within that same layer. Considering the different ofm dimensions, sparsity is 47%.

of convolution kernels. Each activation tensor is a three-dimensional tensor of size  $w \times h \times c$ , where  $w$ ,  $h$  and  $c$  represent the tensor width, height, and depth, respectively. For convenience, the dimensions of  $X_i$  and  $X_o$  are denoted by  $[w_i \times h_i \times c_i]$  and  $[w_o \times h_o \times c_o]$ . Finally, the set of convolution kernels  $W$  is denoted by a four-dimensional tensor  $[k \times k \times c_i \times c_o]$ , where  $k$  is the filter width and height. The filter width and height are not necessarily equal, but it is common practice in most conventional CNNs to take them as such. Given the above notations, each output activation value  $X_o[x, y, z]$  is computed from the input tensor  $X_i$  and weights  $W$  as follows:

$$X_o(x, y, z) = \sum_{i, j=0}^{k-1} \sum_{c=0}^{c_i-1} X_i[x+i, y+j, c] \cdot W[i, j, c, z], \quad (1)$$

where the bias term is omitted for simplicity’s sake. We use the above notations throughout this paper.

### 2.2. Three-Step Method

Conventional convolution layers compute their ofm by applying Equation (1) for each  $[x, y, z]$ . It has been observed that ofms accommodate many zero-valued activations due to the widespread usage of the ReLU activation function. For example, in Figure 2 we present the relative portion of zero-valued activations of ResNet-18 [13] with the ImageNet large scale visual recognition challenge (ILSVRC-2012) dataset [36] — overall, almost 50% of the ofm activations are zero-valued; therefore, 50% of the MAC operations may be potentially skipped. Moreover, ofm activations exhibit spatial correlation [31, 39], meaning that a group of activation values testifies about other adjacent activation values.

We suggest a three-step dynamic prediction mechanism that locates zero-valued ofm activations by exploiting the

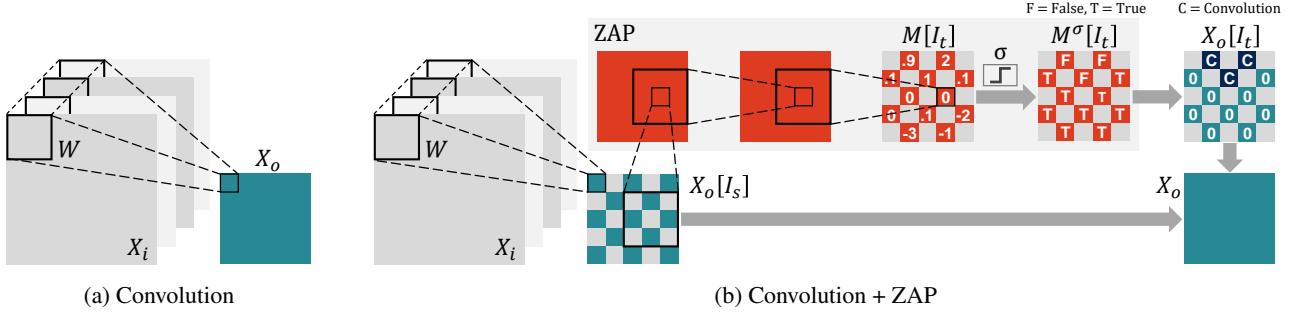


Figure 3: Illustration of a single ofm channel convolution without ZAP (a) and with ZAP (b).  $X_o[I_s]$  is computed based on a pre-defined pattern.  $X_o[I_s]$  is then subjected to ZAP, which produces a prediction map  $M[I_t]$ , followed by a thresholding step to form the binary prediction map  $M^\sigma[I_t]$ .  $X_o[I_t]$  is created according to  $M^\sigma[I_t]$  — a portion of the  $I_t$  ofm activations are predicted as zero-valued and skipped, whereas the rest are computed using Equation (1).

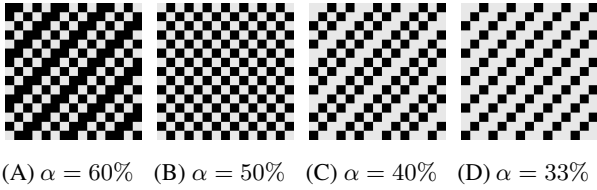


Figure 4: Partial ofm convolution patterns. Black pixels represent computed activations.

spatial correlation inherent in CNNs to potentially skip them and reduce the computational burden of the model. Given an ofm,  $X_o$ , we divide its indices into two subsets ( $I_s, I_t$ ) according to a pre-defined pattern. Then, the following three steps are carried out (as illustrated in Figure 3): (i) the values that belong to indices  $I_s$  are fully computed in the conventional manner, resulting in a sparse ofm,  $X_o[I_s]$ ; (ii) this partial ofm ( $X_o[I_s]$ ) is passed through our predictor to yield a binary map,  $M^\sigma[I_t]$ , which is used to predict the zero values in  $X_o[I_t]$ ; and (iii) all values predicted to be non-zero by  $M^\sigma[I_t]$  are computed. We describe this process in detail next.

**Computation pattern.**  $X_o[I_s]$  is computed based on a pre-defined pattern as depicted in Figure 4. We use  $\alpha$  to denote the ratio between the number of activations computed in the partial ofm and the ofm dimensions. This may be formally formulated as  $\alpha \equiv \frac{|I_s|}{w_o h_o c_o}$ , where  $|I_s|$  is the set cardinality.

By decreasing  $\alpha$ , less ofm activations are computed prior to the prediction, which may potentially lead to the saving of more operations. For example, for  $\alpha = 40\%$ ,  $60\%$  of the activations may potentially be saved. Less prior data about the ofm may, however, lead to higher misprediction rates, which in turn may decrease model accuracy.

**Prediction process via lightweight CNN.** Given the partial ofm,  $X_o[I_s]$ , our goal is to produce an output compu-

tation mask that predicts which of the remaining activations are zero-valued and may be skipped. Recall that ofm activations are originally computed using Equation (1) and so the prediction process must involve less MAC operations than the original convolution operation with as minimal memory footprint as possible.

We use a CNN to implement ZAP. We exploit the spatial correlation inherent in CNNs [31, 39, 20, 8] and use only depthwise convolution (DW-CONV) layers [16], *i.e.*, only spatial filters with no depth ( $k \times k \times 1 \times c_o$ ). As such, we obtain a lightweight model in terms of both MAC operations and parameters (further analyzed in Section 2.3). Our CNN comprises a  $3 \times 3$  DW-CONV layer followed by a batch normalization (BN) layer [19] followed by ReLU, twice. DW-CONV layer padding and stride are both defined as 1 to achieve equal dimensions throughout the CNN predictor. During training, the last ReLU is capped at 1 [22], whereas during inference we discard the last ReLU activation and use a threshold.

**Thresholding.** Although ZAP is trained to output a binary classifier (described in Section 4.1), ZAP naturally outputs  $M[I_t]$ , which is not a strict binary mask but rather a range of values that corresponds to a prediction confidence [10, 45] of whether the ofm activation is zero-valued or not. To binarize ZAP’s output, we define a threshold  $\sigma$  that sets the level of prediction confidence; therefore,  $M^\sigma[I_t] = M[I_t] > \sigma$  (boolean operation).

According to  $M^\sigma[I_t]$ , part of the ofm activations in  $X_o[I_t]$  are predicted to be non-zero-valued and are computed, whereas the others are predicted to be zero-valued and are skipped. When an ofm activation is predicted to be zero-valued, two types of misprediction may occur. First, an actual zero-valued activation may be predicted as a non-zero-valued activation and so redundant MAC operations may take place. Second, an actual non-zero-valued activation may be predicted as zero. The latter misprediction increases the model error, potentially decreasing model ac-

curacy.

The motivation behind ZAP is clear — reducing computations by skipping convolution operations. Its impact on the model accuracy, number of computations, and amount of parameters has yet, however, to be discussed. We next discuss the overhead of ZAP, and in Section 4, we show empirically how ZAP affects the accuracy of different model architectures.

### 2.3. Overhead Analysis

ZAP is a CNN by itself, which means that it introduces additional computations and parameters. To be beneficial, it must execute less operations per ofm activation than the original convolution operation. A conventional convolution layer requires  $k^2 c_i$  MAC operations per ofm activation. On the other hand, the number of MAC operations required by a two-layered DW-CONV ZAP for a single ofm activation is  $K^2$ , where  $K$  is the filter width and height. Note that ZAP’s first layer needs only to consider  $|I_s|$  values for computation since, according to the pre-defined pattern, the remaining  $|I_t|$  values are zero; the second layer needs only to compute  $|I_t|$  ofm activations.

Compared with a standard convolution operation, and for the case of  $K = k$ ,

$$\frac{\text{ZAP ops.}}{\text{standard convolution ops.}} = \frac{1}{c_i}. \quad (2)$$

$c_i$  is usually greater than  $10^2$  [13, 41, 24], in which case  $1/c_i \approx 0$  and ZAP overhead is, therefore, negligible.

Regarding the parameters, a conventional convolution layer requires  $k^2 c_i c_o$  parameters and a two-layered DW-CONV requires  $2K^2 c_o$  parameters. Given  $c_i$  conventional sizes, the standard convolution layer is at least two orders of magnitude larger than ZAP, which means that its memory footprint is negligible as well.

## 3. Accuracy-MAC Savings Trade-Off

The threshold hyperparameter,  $\sigma$ , represents the prediction confidence of whether an ofm activation is zero or non-zero. Users should, however, address the accuracy and MAC reduction terms rather than using  $\sigma$ , since it is not clear how a specific  $\sigma$  value affects accuracy and savings. In this section, we show that, given some statistics, we can estimate the entire model accuracy and predictor MAC savings, thereby avoiding the need to address the threshold value directly.

### 3.1. Accuracy and Threshold

Consider a DNN with  $L$  layers. Each layer  $i$  comprises weights  $w_i$ , an ifm  $x_i$ , and an ofm  $y_i$ . When predictions are avoided, layer  $i + 1$  input,  $x_{i+1}$ , is given by

$$x_{i+1} = y_i = \max(x_i w_i, 0), \quad (3)$$

where  $\max(\cdot, 0)$  is the ReLU activation function.

Our predictor is not perfect and may zero out non-zero elements with a small probability  $\varepsilon_i$ . Therefore, non-zero inputs to layer  $i + 1$  have a probability  $\varepsilon_i$  of becoming zero and a probability  $1 - \varepsilon_i$  of remaining  $y_i$ . Using  $y_i^\pi$  to denote the prediction of output  $y_i$ , we obtain the following error in the expected activation:

$$E(y_i^\pi) = (1 - \varepsilon_i) \cdot E(y_i). \quad (4)$$

In other words, the prediction at each layer  $i$  introduces a multiplicative error of  $(1 - \varepsilon_i)$  with respect to the true activation. This multiplicative error builds up across layers. For an  $L$ -layer network, the expected network outputs are scaled down with respect to the true network outputs as follows:

$$\text{Scale Error} = \prod_{i=1}^L (1 - \varepsilon_i). \quad (5)$$

Note that for a sufficiently small  $\varepsilon$ ,  $1 - \varepsilon = e^{-\varepsilon}$ . Therefore, assuming sufficiently small misprediction probabilities,  $\{\varepsilon_i\}$ , we obtain the following expression

$$\begin{aligned} \text{Scale Error} &= \prod_{i=1}^L (1 - \varepsilon_i) \approx \prod_{i=1}^L e^{-\varepsilon_i} \\ &= e^{-\sum_{i=1}^L \varepsilon_i} \approx 1 - \sum_{i=1}^L \varepsilon_i, \end{aligned} \quad (6)$$

where the approximations can easily be extracted from a Taylor expansion to  $e^{-x}$ . Equation (6) shows that the final error due to small mispredictions accumulates along the network in a *linear* fashion when the errors due to mispredictions are small enough.

Denoting the output of layer  $i$  for a threshold  $\sigma$  by  $y_i^{\pi, \sigma}$ , the error is associated with a threshold  $\sigma$  as follows:

$$\begin{aligned} \text{Scale Error}(\sigma) &\approx 1 - \sum_{i=1}^L \varepsilon_i(\sigma) \\ &= 1 - \sum_{i=1}^L \left( 1 - \frac{\sum_{x,y,z} y_i^{\pi, \sigma}[x, y, z]}{\sum_{x,y,z} y_i[x, y, z]} \right), \end{aligned} \quad (7)$$

where Equation (4) is used for the last transition. Figure 5 shows that this analytical observation is in good agreement with our empirical results.

Ideally, we would like to have a scale error that is as close as possible to 1 so as to avoid shifting the network statistics from the learned distribution. When the scale error is 1, network outputs remain unchanged and no accuracy degradation associated with mispredictions occurs. Yet, as  $\sigma$  increases, more ofm activations are predicted as zero-valued, decreasing the scale error below 1, as exhibited by Equation (7). This scale error decreases monotonically with  $\sigma$ .

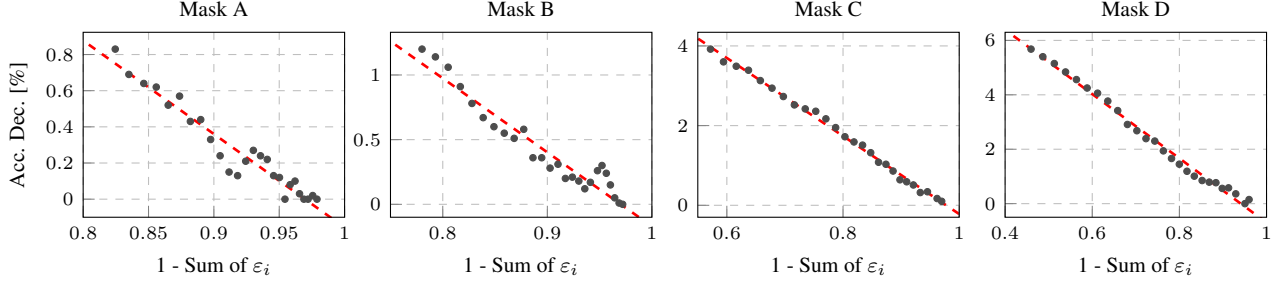


Figure 5: AlexNet + CIFAR-100 top-1 accuracy decrease as a function of  $1 - \sum_{i=1}^L \varepsilon_i(\sigma)$ . Each dot represents a measurement with a different threshold: the leftmost and rightmost thresholds are 0 and 0.5, respectively. Measurements were taken in steps of 0.02.

and introduces an inverse mapping, which enables us to define a threshold value for any desired accuracy degradation.

At this point, given the model accuracy-error linearity and the error to threshold transformation, we have a transformation from accuracy to threshold and vice versa. Next we discuss the relationship between MAC savings and  $\sigma$ .

### 3.2. MAC Savings and Threshold

In this subsection, we quantify the MAC reductions for a certain layer. Clearly, the total MAC reduction equals the sum of the contributions from all layers. Recall that  $M[I_t]$  represents the collection of values predicted by ZAP before applying the threshold. Assume a discrete distribution with frequency densities  $\{p(x_i)\}$  for the values in  $M[I_t]$ , where each value  $x_i$  represents an interval (bin) of equal width in the range  $[\min(M[I_t]), \max(M[I_t])]$ . Then, MAC savings relative to total MAC operations can be expressed as follows:

$$\text{Zero Prediction Rate } (\sigma) = \sum_{i=0}^k p(x_i), \quad (8)$$

where  $x_{k-1} \leq \sigma \leq x_k$ .

Each predicted zero, whether correct or not, leads to a MAC reduction. Equation (2) shows that each predicted zero reduces the MAC calculation by a factor of  $\frac{1}{c_i}$ . Then, MAC savings relative to total MAC operations can be expressed as follows:

$$\text{MAC Reduction } (\sigma) = \frac{\text{Zero Prediction Rate } (\sigma) \cdot \frac{1}{c_i}}{w_o h_o c_o}. \quad (9)$$

Note that MAC reduction as a function of  $\sigma$  increases monotonically, and for a certain range it may be considered a strictly monotonic function; therefore, inverse mapping from MAC reduction to  $\sigma$  is possible, as depicted in Figure 6.

### 3.3. Trade-off Control

In Subsections 3.1 and 3.2, we showed how to make an *a priori* choice of any operating point, given estimates about

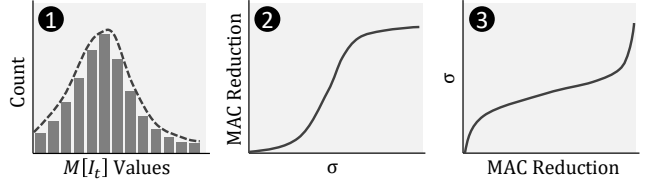


Figure 6: The transformation process from a prediction values histogram (or distribution) to the threshold versus MAC reduction curve.

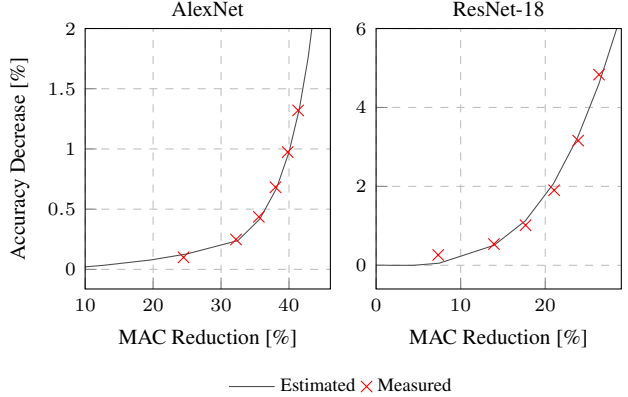


Figure 7: Estimated top-5 accuracy-MAC savings trade-off curve using Mask B and ILSVRC-2012 dataset. The measured operating points correspond to thresholds of 0 to 0.5, in steps of 0.1.

the desired accuracy and MAC reduction, without dealing with the threshold. We assume a pre-processing step that consists of collecting statistical information about the prediction values  $M[I_t]$  and at least two accuracy measurements of the entire model to obtain the linear accuracy-error relationship. With this statistical information, we can effectively estimate the desired operating point, as demonstrated in Figure 7.

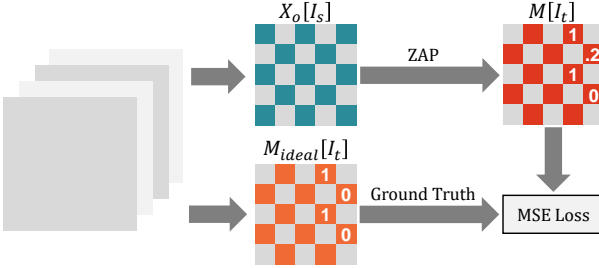


Figure 8: Illustration of the training of a single ZAP. The ground truth is the original layer of fm after a binary threshold operation ( $>0$ ). The CNN predictor is used with the ReLU activation function capped at 1.

## 4. Experiments

In this section, we evaluate ZAP performance in terms of MAC savings and accuracy degradation using various model architectures and datasets, and compare our results to previous work.

### 4.1. ZAP Training

ZAPs are deployed at each desired convolution layer and are trained independently. By training in isolation [14, 7], ZAPs can be plugged into a model without altering its architecture and trained parameters and may be trained in parallel. First, a batch is fed forward bypassing all predictors. During the feedforward phase, each ZAP saves a copy of its local input feature map (ifm) and corresponding local ofm. Then, each ZAP computes its  $M[I_t]$ , using its ifm followed by a ReLU activation function which is capped at 1. The ground truth,  $M_{ideal}$ , of each ZAP is its local ofm passed through a zero-threshold boolean operation at indices  $I_t$ . Finally, the MSE loss is used to minimize each of the predictor errors, as follows:

$$\min \sum_{(x,y,z) \in I_t} (M - M_{ideal})^2. \quad (10)$$

ZAP training is illustrated in Figure 8.

### 4.2. Experimental Setup

We evaluated our method using CIFAR-100 [23] and ILSVRC-2012 [36] datasets, and AlexNet [24], VGG-16 [41], and ResNet-18 [13] CNN architectures. PyTorch 1.1.0 [34] was used as our deep learning framework. The source code is publicly available<sup>1</sup>.

ZAPs were trained using the Adam [21] optimizer for 5 epochs. When using the ILSVRC-2012 dataset, only 32K training set images were used. After ZAPs were trained, we recalibrated the running mean and variance of the model BN

layers; this is not considered fine-tuning since it does not involve backpropagation. BN recalibration was noticeably important with ResNet-18, which has multiple BN layers. When fine-tuning was considered, it was limited to 5 epochs with CIFAR-100 and to 1 epoch with ILSVRC-2012. The models were fine-tuned using their original hyperparameters with the smallest learning rate values. We did not deploy ZAPs on the first layers of any of the models, since such deployment is not beneficial in terms of potential operation savings.

AlexNet with CIFAR-100 was trained from scratch using the original hyperparameters, achieving top-1 accuracy of 64.4%. AlexNet, VGG-16, and ResNet-18 with ILSVRC-2012 were used with the PyTorch pretrained parameters, achieving top-1/top-5 accuracies of 56.5%/79.1%, 71.6%/90.6%, and 69.8%/89.1%, respectively.

We experimented with four different prediction patterns (Figure 4). The same prediction pattern was used across all layers and channels. Mixing patterns in layer and channel granularity is an option that we leave for future work.

Throughout this section, MAC reduction is defined as  $(1 - \text{after/before})$  and accuracy degradation is defined as  $(\text{before} - \text{after})$ . When discussing MAC reduction, we consider only the relative savings from convolution layers.

### 4.3. CIFAR-100

**Operating points.** We demonstrate different operating points as measured with different masks and thresholds with AlexNet using the CIFAR-100 dataset. For each operating point, we report the entire model top-1 accuracy degradation and MAC operation savings, with and without fine-tuning (Figure 9). For example, considering a 1% top-1 accuracy degradation cap, ZAP achieves a 32.4% MAC reduction with 0.7% accuracy degradation at Mask B with a 0.4 threshold. In addition, by fine-tuning the model, our predictor achieves 40.3% MAC reduction with 0.8% accuracy degradation at Mask D with a 0.3 threshold.

Masks with greater  $\alpha$  values lead to ofms with relatively more computed activations, *i.e.*, larger  $|I_s|$ . We observe that these masks show better accuracy results in the low degradation region (*e.g.*, Mask A versus Mask D at 20% MAC reduction), whereas for higher MAC reduction requirements, masks with lower  $\alpha$  values are preferred. In order to achieve high MAC reductions with the former masks (for example, mask A),  $\sigma$  would have to be cranked up. Since the prediction potential of these masks is low to begin with (for example, the best-case scenario with Mask A is 40% activations savings with mask A), high thresholds will lead to pruning of relatively significant values and, as a result, to significant accuracy degradation. On the other hand, for conservative MAC reductions, these masks are preferred, since their speculation levels are lower and prediction confidence is higher.

<sup>1</sup><https://github.com/gilshm/zap>

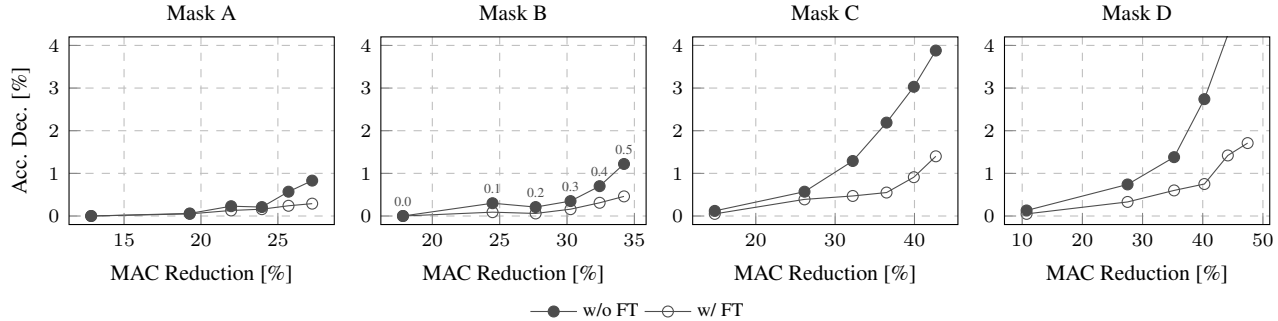


Figure 9: Demonstrating the different operating points of AlexNet + CIFAR-100 with (w/) and without (w/o) fine-tuning (FT). Accuracy measurements are top-1. Threshold range is set between 0 to 0.5, in steps of 0.1. Each measurement corresponds to a threshold, as presented in “Mask B” plot.

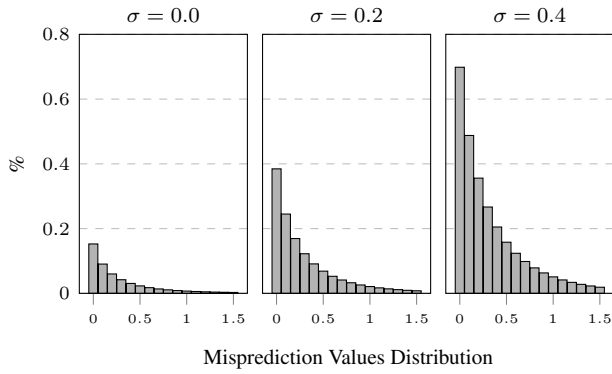


Figure 10: AlexNet + CIFAR-100 histograms of non-zero values that were predicted as zero using Mask B and different thresholds.

**Misprediction breakdown.** The model accuracy is not solely dependent on *how many* non-zeros were predicted as zero, but also *which* values were zeroed out. The notion that small values within DNN are relatively ineffectual is at the core of many pruning techniques. In Figure 10 we present the mispredicted activation values distribution, normalized to the number of ofm activations for value steps of 0.1. For example, when using  $\sigma = 0$ , 0.15% of ofm activations with original values between 0 to 0.1 were zeroed out. Increasing the threshold level increases the number of predicted and mispredicted ofm activations. It is apparent that insignificant values are more prone to be mispredicted — it is easier to be mistaken about zeroing out a small value than a large value — attesting to the correlation between  $\sigma$  and the prediction confidence level.

#### 4.4. ILSVRC-2012

**Estimated operating points.** In Figure 7 we demonstrated how the entire accuracy to MAC reduction curve can be estimated for AlexNet and ResNet-18 with the ILSVRC-

2012 dataset without retraining and using Mask B. From these curves, the user may choose a desired operating point. For example, given a 1% top-5 accuracy decrease cap, ZAP provides 40% and 17.5% MAC operations savings for AlexNet and ResNet-18, respectively.

**Comparison with previous work.** In Table 1 we compare our method with the work of Figurnov *et al.* [8], Kim *et al.* [20], Shomron and Weiser [39], and Dong *et al.* [6]. Using AlexNet and VGG-16, our method shows better results across the board: for the same accuracy, more MAC savings are achieved, and for the same MAC savings, a smaller accuracy drop is observed. Regarding ResNet-18, our method shows significantly better accuracy results without fine-tuning, compared to Shomron and Weiser. With fine-tuning, however, Shomron and Weiser achieved slightly better results for the top-1 case. Dong *et al.* achieved great results, but their method involves an entire network training with *hundreds* of epochs. Therefore, even though there is a resemblance between our method and theirs, the results are not necessarily comparable.

## 5. Related Work

**Speculative execution.** General-purpose processors (GPPs) make extensive use of speculative execution of actions [15]. For example, branch predictors are used to predict whether a branch instruction will be taken (or not taken) based on previous encounters with that branch or other nearby branches, and caches are used to store values that will probably be accessed repetitively in the near future. These speculative mechanisms leverage unique application characteristics, such as code semantics and temporal locality, to better utilize the GPP’s internal structure to achieve better performance.

Researchers have also studied the speculative execution of CNNs to decrease their compute demands. Akhlaghi *et al.* [1] predict during the convolution computation whether the convolution results will end up negative. Song *et al.*

| Network   | Paper                  | Related Work |            |      |            |              | Ours        |             |             |             |              |
|-----------|------------------------|--------------|------------|------|------------|--------------|-------------|-------------|-------------|-------------|--------------|
|           |                        | Top1         | Top1-ft    | Top5 | Top5-ft    | MAC          | Top1        | Top1-ft     | Top5        | Top5-ft     | MAC          |
| AlexNet   | Figurnov <i>et al.</i> | -            | -          | 8.50 | 2.0        | 50.0%        | 4.41        | 1.91        | <b>2.89</b> | <b>1.29</b> | <b>51.6%</b> |
|           | Kim <i>et al.</i>      | 0.48         | -          | 0.40 | -          | 28.6%        | <b>0.44</b> | 0.35        | <b>0.25</b> | 0.17        | <b>32.2%</b> |
|           | Shomron and Weiser     | 4.00         | 1.6        | 2.90 | 1.3        | 37.8%        | <b>1.01</b> | <b>0.86</b> | <b>0.68</b> | <b>0.29</b> | <b>38.0%</b> |
| VGG-16    | Figurnov <i>et al.</i> | -            | -          | 15.6 | 1.1        | 44.4%        | 10.0        | 1.66        | <b>5.92</b> | <b>0.98</b> | <b>44.6%</b> |
|           | Kim <i>et al.</i>      | 0.68         | -          | 0.26 | -          | 25.7%        | <b>0.43</b> | 0.13        | <b>0.23</b> | 0.08        | <b>29.0%</b> |
|           | Shomron and Weiser     | 3.60         | 0.7        | 2.00 | 0.4        | 30.7%        | <b>1.01</b> | <b>0.24</b> | <b>0.55</b> | <b>0.09</b> | <b>32.3%</b> |
| ResNet-18 | Dong <i>et al.</i> *   | -            | <b>3.6</b> | -    | <b>2.3</b> | <b>34.6%</b> | 6.39        | 4.15        | 4.00        | 2.45        | 25.2%        |
|           | Shomron and Weiser     | 11.0         | <b>2.7</b> | 7.60 | <b>1.7</b> | 22.7%        | <b>4.65</b> | 2.96        | <b>2.69</b> | <b>1.70</b> | <b>23.1%</b> |

Table 1: MAC reduction and accuracy with and without fine-tuning (ft) — our results compared with previous work. The accuracy columns represent the decrease in accuracy. The MAC columns represent the MAC operations reduction. The minus (‘-’) symbol represents unpublished data.

[42], Lin *et al.* [29], and Chang *et al.* [4] predict whether an entire convolution result is negative according to a partial result yielded by the input MSB bits. Huan *et al.* [18] avoid convolution multiplications by predicting and skipping near-zero valued data, given certain thresholds. Chen *et al.* [5] predict future weight updates during training based on Momentum [35] parameters. Zhu *et al.* [46] use a fully connected layer to predict each ofm activation sign and low-rank approximation to decrease the weight matrix.

In conventional GPPs, control and data mispredictions may lead to a pipeline flush and a rewind of the program counter, *i.e.*, it is common that an execution stops and starts over due to mispredictions. Interestingly, this is not the case with DNNs, since they are statistics-based and tolerant to errors (to some extent) [26]. Therefore, the impact of mispredictions on the model accuracy depends on *how many* non-zero-valued activations are predicted as zero, as well as on *which* values were zeroed out.

**Spatial correlation.** The correlation between neighboring activations in CNN feature maps is an inherent CNN characteristic that may be exploited. Shomron and Weiser [39], Kim *et al.* [20], and Figurnov *et al.* [8] partially compute the ofmap activations and interpolate the rest. Shomron and Weiser, and Kim *et al.* focus on predicting zero-valued activations whereas Figurnov *et al.* mainly use “nearest neighbor” to interpolate missing values. Finally, Mahmoud *et al.* [31] operate on reduced precision deltas between adjacent activations rather than on true values.

**Dynamic pruning.** As opposed to static pruning [12, 17, 30, 30, 27], dynamic pruning is input-dependent, *i.e.*, part of the network may be skipped depending on the current inputs. Dong *et al.* [6] present a network structure with embedded low-cost convolution layers that act as zero-valued activation masks for the original convolution masks. Lin *et al.* [28] use reinforcement learning for channel pruning. Gao *et al.* [9] create a channel saliency map by subsampling the ifm followed by a fully connected layer from which they pick the pruned channels, and He *et al.* [14] propose a two-

step channel pruning algorithm with LASSO regression and fine-tuning of weights.

**Network for network.** Conceptually, our work demonstrates how a NN is used for the benefit of another NN and so it may relate to neural architecture search (NAS) work, a field in which model architectures are formed automatically by another network [47, 44]. In addition, some works on dynamic pruning also share this concept [9, 28], as mentioned previously.

Our work is most closely related to the work of Dong *et al.*, Shomron and Weiser, Kim *et al.*, and Figurnov *et al.*, with which we have also compared our results. As opposed to Dong *et al.*, our approach is easy to deploy, *i.e.*, it does not require training of the entire model and it offers the user many operating points to choose from. In addition, our prediction mask relies on partial ofm computation rather than on the ifm. As for Shomron and Weiser, Kim *et al.*, and Figurnov *et al.*, we create binary prediction masks using a CNN-based approach and offer an estimate of the model accuracy degradation and MAC savings.

## 6. Conclusions

In this paper, we propose a zero activation predictor (ZAP) that dynamically identifies the zero-valued output feature map (ofm) activations prior to their computation, thereby saving their convolution operations. ZAP exploits the spatial correlation of ofm activations inherent in convolution neural networks, meaning that according to a sparsely computed ofm, ZAP determines whether the remaining activations are zero-valued or non-zero-valued. ZAP is a lightweight CNN that imposes negligible computation and parameter overheads and its deployment and training does not require a modification of the baseline model architecture and parameters. In addition, ZAP speculation level is tunable, allowing an efficient *a priori* control of the accuracy-savings trade-off.

## Acknowledgments

We gratefully acknowledge the support of NVIDIA Corporation and its donation of the Titan V GPU used for this research.

## References

- [1] Vahideh Akhlaghi, Amir Yazdanbakhsh, Kambiz Samadi, Rajesh K Gupta, and Hadi Esmaeilzadeh. SnaPEA: Predictive early activation for reducing computation in deep convolutional neural networks. In *International Symposium on Computer Architecture (ISCA)*, pages 662–673. IEEE, 2018.
- [2] Jorge Albericio, Patrick Judd, Tayler Hetherington, Tor Aamodt, Natalie Enright Jerger, and Andreas Moshovos. Cnvlutin: Ineffectual-neuron-free deep neural network computing. In *International Symposium on Computer Architecture (ISCA)*, pages 1–13. IEEE, 2016.
- [3] Alfredo Canziani, Adam Paszke, and Eugenio Culurciello. An analysis of deep neural network models for practical applications. *arXiv preprint arXiv:1605.07678*, 2016.
- [4] Jiho Chang, Yoonsung Choi, Taegyoung Lee, and Junhee Cho. Reducing MAC operation in convolutional neural network with sign prediction. In *International Conference on Information and Communication Technology Convergence (ICTC)*, pages 177–182. IEEE, 2018.
- [5] Chi-Chung Chen, Chia-Lin Yang, and Hsiang-Yun Cheng. Efficient and robust parallel dnn training through model parallelism on multi-gpu platform. *arXiv preprint arXiv:1809.02839*, 2018.
- [6] Xuanyi Dong, Junshi Huang, Yi Yang, and Shuicheng Yan. More is less: A more complicated network with less inference complexity. In *Conference on Computer Vision and Pattern Recognition (CVPR)*, pages 5840–5848. IEEE, 2017.
- [7] Ahmed T Elthakeb, Prannoy Pilligundla, and Hadi Esmaeilzadeh. Divide and conquer: Leveraging intermediate feature representations for quantized training of neural networks. *International Conference on Machine Learning (ICML) Workshop on Understanding and Improving Generalization in Deep Learning*, 2019.
- [8] Mikhail Figurnov, Aizhan Ibraimova, Dmitry P Vetrov, and Pushmeet Kohli. PerforatedCNNs: Acceleration through elimination of redundant convolutions. In *Advances in Neural Information Processing Systems (NIPS)*, pages 947–955, 2016.
- [9] Xitong Gao, Yiren Zhao, Lukasz Dudziak, Robert Mullins, and Cheng-zhong Xu. Dynamic channel pruning: Feature boosting and suppression. *International Conference on Learning Representations (ICLR)*, 2018.
- [10] Yonatan Geifman and Ran El-Yaniv. Selective classification for deep neural networks. In *Advances in Neural Information Processing Systems (NIPS)*, pages 4878–4887, 2017.
- [11] Song Han, Xingyu Liu, Huizi Mao, Jing Pu, Ardavan Pedram, Mark A Horowitz, and William J Dally. EIE: efficient inference engine on compressed deep neural network. In *International Symposium on Computer Architecture (ISCA)*, pages 243–254. IEEE, 2016.
- [12] Song Han, Huizi Mao, and William J Dally. Deep compression: Compressing deep neural networks with pruning, trained quantization and huffman coding. In *International Conference on Learning Representations (ICLR)*, 2016.
- [13] Kaiming He, Xiangyu Zhang, Shaoqing Ren, and Jian Sun. Deep residual learning for image recognition. In *Conference on Computer Vision and Pattern Recognition (CVPR)*, pages 770–778. IEEE, 2016.
- [14] Yihui He, Xiangyu Zhang, and Jian Sun. Channel pruning for accelerating very deep neural networks. In *International Conference on Computer Vision (ICCV)*, pages 1389–1397. IEEE, 2017.
- [15] John L Hennessy and David A Patterson. *Computer architecture: a quantitative approach*. Elsevier, 2011.
- [16] Andrew G Howard, Menglong Zhu, Bo Chen, Dmitry Kalenichenko, Weijun Wang, Tobias Weyand, Marco Andreetto, and Hartwig Adam. MobileNets: Efficient convolutional neural networks for mobile vision applications. *arXiv preprint arXiv:1704.04861*, 2017.
- [17] Hengyuan Hu, Rui Peng, Yu-Wing Tai, and Chi-Keung Tang. Network trimming: A data-driven neuron pruning approach towards efficient deep architectures. *arXiv preprint arXiv:1607.03250*, 2016.
- [18] Yuxiang Huan, Yifan Qin, Yantian You, Lirong Zheng, and Zhuo Zou. A multiplication reduction technique with near-zero approximation for embedded learning in IoT devices. In *International System-on-Chip Conference (SOCC)*, pages 102–107. IEEE, 2016.
- [19] Sergey Ioffe and Christian Szegedy. Batch normalization: Accelerating deep network training by reducing internal covariate shift. *International Conference on Machine Learning (ICML)*, 2015.
- [20] Cheolhwan Kim, Dongyeob Shin, Bohun Kim, and Jongsun Park. Mosaic-CNN: A combined two-step zero prediction approach to trade off accuracy and computation energy in convolutional neural networks. *Journal on Emerging and Selected Topics in Circuits and Systems*, 8(4):770–781, 2018.
- [21] Diederik P Kingma and Jimmy Ba. Adam: A method for stochastic optimization. *International Conference on Learning Representations (ICLR)*, 2014.
- [22] Alex Krizhevsky and Geoff Hinton. Convolutional deep belief networks on CIFAR-10. *Unpublished manuscript*, 40(7):1–9, 2010.
- [23] Alex Krizhevsky, Vinod Nair, and Geoffrey Hinton. CIFAR-10 and CIFAR-100 datasets. <http://www.cs.toronto.edu/~kriz/cifar.html>.
- [24] Alex Krizhevsky, Ilya Sutskever, and Geoffrey E Hinton. ImageNet classification with deep convolutional neural networks. In *Advances in Neural Information Processing Systems (NIPS)*, pages 1097–1105, 2012.
- [25] Sergey Levine, Chelsea Finn, Trevor Darrell, and Pieter Abbeel. End-to-end training of deep visuomotor policies. *Journal of Machine Learning Research*, 17(1):1334–1373, 2016.
- [26] Guanpeng Li, Siva Kumar Sastry Hari, Michael Sullivan, Timothy Tsai, Karthik Pattabiraman, Joel Emer, and Stephen W Keckler. Understanding error propagation in

deep learning neural network (DNN) accelerators and applications. In *International Conference for High Performance Computing, Networking, Storage and Analysis (SC)*, page 8. ACM, 2017.

[27] Hao Li, Asim Kadav, Igor Durdanovic, Hanan Samet, and Hans Peter Graf. Pruning filters for efficient ConvNets. In *International Conference on Learning Representations (ICLR)*, 2017.

[28] Ji Lin, Yongming Rao, Jiwen Lu, and Jie Zhou. Runtime neural pruning. In *Advances in Neural Information Processing Systems (NIPS)*, pages 2181–2191, 2017.

[29] Yingyan Lin, Charbel Sakr, Yongjune Kim, and Naresh Shanbhag. PredictiveNet: An energy-efficient convolutional neural network via zero prediction. In *International Symposium on Circuits and Systems (ISCAS)*, pages 1–4. IEEE, 2017.

[30] Jian-Hao Luo, Jianxin Wu, and Weiyao Lin. ThiNet: A filter level pruning method for deep neural network compression. In *International Conference on Computer Vision (ICCV)*, pages 5058–5066. IEEE, 2017.

[31] Mostafa Mahmoud, Kevin Siu, and Andreas Moshovos. Diffy: a déjà vu-free differential deep neural network accelerator. In *International Symposium on Microarchitecture (MICRO)*, pages 134–147. IEEE, 2018.

[32] Vinod Nair and Geoffrey E Hinton. Rectified linear units improve restricted boltzmann machines. In *International Conference on Machine Learning (ICML)*, pages 807–814, 2010.

[33] Angshuman Parashar, Minsoo Rhu, Anurag Mukkara, Antonio Puglielli, Rangharajan Venkatesan, Brucek Khailany, Joel Emer, Stephen W Keckler, and William J Dally. SCNN: An accelerator for compressed-sparse convolutional neural networks. In *International Symposium on Computer Architecture (ISCA)*, pages 27–40. IEEE, 2017.

[34] Adam Paszke, Sam Gross, Soumith Chintala, Gregory Chanan, Edward Yang, Zachary DeVito, Zeming Lin, Alban Desmaison, Luca Antiga, and Adam Lerer. Automatic differentiation in PyTorch. In *Advances in Neural Information Processing Systems (NIPS) Autodiff Workshop*, 2017.

[35] Ning Qian. On the momentum term in gradient descent learning algorithms. *Neural Networks*, 12(1):145–151, 1999.

[36] Olga Russakovsky, Jia Deng, Hao Su, Jonathan Krause, Sanjeev Satheesh, Sean Ma, Zhiheng Huang, Andrej Karpathy, Aditya Khosla, Michael Bernstein, et al. ImageNet large scale visual recognition challenge. *International Journal of Computer Vision (IJCV)*, 115(3):211–252, 2015.

[37] Tara N Sainath, Abdel-rahman Mohamed, Brian Kingsbury, and Bhuvana Ramabhadran. Deep convolutional neural networks for LVCSR. In *International Conference on Acoustics, Speech and Signal Processing (ICASSP)*, pages 8614–8618. IEEE, 2013.

[38] Gil Shomron, Tal Horowitz, and Uri Weiser. SMT-SA: Simultaneous multithreading in systolic arrays. *Computer Architecture Letters (CAL)*, 18(2):99–102, 2019.

[39] Gil Shomron and Uri Weiser. Spatial correlation and value prediction in convolutional neural networks. *Computer Architecture Letters (CAL)*, 18(1):10–13, 2019.

[40] David Silver, Aja Huang, Chris J Maddison, Arthur Guez, Laurent Sifre, George Van Den Driessche, Julian Schrittwieser, Ioannis Antonoglou, Veda Panneershelvam, Marc Lanctot, et al. Mastering the game of Go with deep neural networks and tree search. *Nature*, 529(7587):484, 2016.

[41] Karen Simonyan and Andrew Zisserman. Very deep convolutional networks for large-scale image recognition. *International Conference on Machine Learning (ICML)*, 2015.

[42] Mingcong Song, Jiechen Zhao, Yang Hu, Jiaqi Zhang, and Tao Li. Prediction based execution on deep neural networks. In *International Symposium on Computer Architecture (ISCA)*, pages 752–763. IEEE, 2018.

[43] Vivienne Sze, Yu-Hsin Chen, Tien-Ju Yang, and Joel S Emer. Efficient processing of deep neural networks: A tutorial and survey. *Proceedings of the IEEE*, 105(12):2295–2329, 2017.

[44] Mingxing Tan, Bo Chen, Ruoming Pang, Vijay Vasudevan, Mark Sandler, Andrew Howard, and Quoc V Le. MnasNet: Platform-aware neural architecture search for mobile. In *Conference on Computer Vision and Pattern Recognition (CVPR)*, pages 2820–2828, 2019.

[45] Reza Yazdani, Marc Riera, Jose-Maria Arnaud, and Antonio González. The dark side of DNN pruning. In *International Symposium on Computer Architecture (ISCA)*, pages 790–801. IEEE, 2018.

[46] Jingyang Zhu, Jingbo Jiang, Xizi Chen, and Chi-Ying Tsui. Sparsenn: An energy-efficient neural network accelerator exploiting input and output sparsity. In *Design, Automation and Test in Europe Conference (DATE)*, pages 241–244. IEEE, 2018.

[47] Barret Zoph and Quoc V Le. Neural architecture search with reinforcement learning. In *International Conference on Learning Representations (ICLR)*, 2017.